



# Entropy Generation and Optimization of Laminar Forced Convection Air Cooling in a Horizontal Channel Containing Heated Sources

M. Bensouici<sup>1†</sup> and, F. Z. Bensouici<sup>2</sup>

<sup>1</sup> *Laboratory of Applied Energetics and Pollution, Faculty of Engineering Sciences, Department of Mechanical Engineering, University of Mentouri Brothers-Constantine, Road of Ain El. Bey, Constantine 25000, Algeria*

<sup>2</sup> *Faculty of Pharmaceutical Process Engineering, University of Constantine 3, UV N05, Ali Mendjeli New City, Khroub, Constantine 25000, Algeria*

†Corresponding Author Email: [moumtezbensouici1977@gmail.com](mailto:moumtezbensouici1977@gmail.com)

(Received June 29, 2016; accepted December 26, 2016)

## ABSTRACT

A forced convection air-cooling of two identical heat sources mounted in a horizontal channel is numerically studied. Four effects of Reynolds number, separation distance, height and width of the components on the flow structure and heat transfer inside the channel have been examined. The entropy generation minimization method (EGM) is employed to optimize the heat transfer and fluid flow in the channel. The flow field is governed by the Navier–Stokes equation and the thermal field by the energy equation. The finite volume method and the SIMPLER algorithm are used to solve the continuity, momentum, energy and entropy generation equations. Results show that the mean Nusselt number increases with increase of the following parameters: Reynolds number, separation distance, height and width of the components. However, these parameters increase the total entropy generation, and thus provokes the degradation of the fan energy. The optimal values of separation distance, height and width heat source are: [( $S_{opt}=1$  with  $W=0.25$ ,  $C=0.25$ ,  $Re=50$ ,  $\eta=1.134$ ), ( $C_{opt}=0.3$  with  $W=0.25$ ,  $S=0.25$ ,  $Re=100$ ,  $\eta=0.895$ ) and ( $W_{opt}=0.1$   $S=0.25$ ,  $C=0.25$ ,  $Re=200$ ,  $\eta=1.004$ )], respectively, where  $\eta$  is the optimization factor ( $=Num/S_T^*$ ) and is defined as the ratio of Nusselt number to the total entropy generation. Finally, the optimal and the best configuration for maximum heat transfer and minimum entropy generation is observed at  $Re=50$ ,  $S=1$ ,  $C=0.25$  and  $W=0.25$ .

**Keywords:** Numerical simulation; Forced convection; Electronic component cooling; Entropy generation analysis; Optimization procedure.

## NOMENCLATURE

Be	Bejan number	Pr	fluid Prandtl number
c	height of the heat source	Re	Reynolds number
C	dimensionless height of the heat source	s	spacing between the heat sources
H	channel height	S	dimensionless spacing between the blocks
$k_f$	thermal conductivity of the fluid	$S_{l,f}$	local volumetric entropy generation in flow due to the fluid friction
$k_s$	thermal conductivity of the solid	$S_{l,h,t}$	local volumetric entropy generation in flow due to the heat transfer
$k^*$	dimensionless thermal conductivity	$S_{lff}^*$	dimensionless local entropy generation in flow due to the fluid friction
l	channel length	$S_{lht}^*$	dimensionless local entropy generation in flow due to the heat transfer
$l_{in}$	entrance length	$S^*$	dimensionless local total entropy generation due to the fluid friction and heat transfer
$l_{out}$	length after the last heat source	$S_T^*$	dimensionless total entropy generation
L	dimensionless channel length	T	temperature
$L_{in}$	dimensionless entrance length		
$L_{out}$	dimensionless length after the last block		
n	normal of the block surface		
Nu	local Nusselt number		
Num	mean Nusselt number		
p	pressure		
P	dimensionless pressure		

$T_0$	inlet temperature
$u$	x-component velocity
$v$	y-component velocity
$U$	dimensionless x-component velocity
$V$	dimensionless y-component velocity
$U_0$	inlet velocity
$w$	width of the heat source
$W$	dimensionless width of the heat source
$x$	horizontal coordinate
$y$	vertical coordinate
$X$	dimensionless horizontal coordinate
$Y$	dimensionless vertical coordinate
$\alpha_f$	thermal diffusivity of the fluid

$\eta$	optimization factor
$\rho_f$	density of the fluid
$\mu_f$	dynamic viscosity of the fluid
$\nu_f$	kinematic viscosity of the fluid
$\nu^*$	dimensionless kinematic viscosity
$\phi$	irreversibility distribution ratio
$\Theta$	dimensionless temperature Superscript
*	dimensionless quantity

#### Subscripts

s	source
f	fluid
0	reference value
opt	optimal

## 1. INTRODUCTION

In the objective to improve electronic component cooling, a several numeric and experimental research works have been achieved. These works are classified in three research axes that are: natural, forced and mixed convection. Afrid and Zebib (1989) numerically simulated natural convection from cooling of heated blocks mounted on a vertical wall. They found that increasing the spacing between the blocks produces a better cooling of blocks. Davalath and Bayazitoglu (1987) studied the laminar forced convection over an array of heat generating rectangular blocks. They showed that the vertical faces of the heat generating blocks are not efficiently cooled. Bensouici and Bessaïh (2010) studied the mixed convection air-cooling of two identical heat sources mounted in a vertical channel by using a porous matrix. Results show that a better cooling is obtained for the channel completely filled with a porous material, except the components, with the Richardson number ( $Ri = Gr/Re^2 = 0.25$ ), where  $Gr = 10^4$  is the Grashof number and  $Re = 200$  is the Reynolds number, and for all Darcy numbers ( $10^{-5} \leq Da \leq 10^{-3}$ ).

The fan energy transmitted to the fluid flow is dissipated along the channel. The fluid friction and heat transfer are the cause of this dissipation. The fluid friction is due to the airflow and the heat transfer is due to the thermal gradient between the ambient air and the heat source. Therefore, it is imperative to study the performance of the electronic component cooling, by studying the variation of the entropy generation of the system (fluid), and to try to minimize it, what we call it the entropy generation minimization (EGM) method. The method of entropy generation minimization (EGM), established by Bejan (1994), and that is applied to several industrial applications such as heat exchangers and solar power system. The entropy generation minimization (EGM) method permits to optimize the energy of the system.

Magherbi *et al.* (2003) analyzed the entropy generation due to heat transfer and fluid friction in transient state for laminar natural convection in a square cavity. For a natural convection in  $\Gamma$ -shaped enclosures, Dagtekin *et al.* (2007) found that for Ra numbers ranging from  $10^3$  to  $10^4$ , the total entropy

generation (EG) is mostly due to heat transfer, because of relatively low velocities, but for  $Ra > 10^4$ , the contribution due to fluid friction becomes effective, even has comparable values from  $Ra = 10^5$  to  $Ra = 10^6$ . Abbassi *et al.* (2003) investigated the entropy generation in Poiseuille–Benard channel flow. Results show that the maximum entropy generation is localized at areas, where heat exchanged between the walls and the flow is maximum. No significant entropy production is seen in the main flow. Using FLUENT 6.2 code, Balaji *et al.* (2007) presented a numerical investigation of turbulent mixed convection from a symmetrically heated vertical channel, bathed by a steady upward flow of cold air. They give the optimum conditions, where the ratio of the entropy generation due to fluid friction to total entropy generation rate varies within a narrow band (0.14–0.22).

Jian-hui *et al.* (2009) analyzed the entropy generation Minimization rate of the plate-finned heat sinks using computational fluid dynamics and combined optimization. They developed two correlations describing Nusselt number Nu, as well as friction factor f as the functions of geometrical and operational parameters, fin spacing (s), fin thickness (t), and Reynolds number (Re), when the entropy generation rate reaches the lowest value. Shuja *et al.* (2008) studied the effects of channel inlet port height, porosity, and block aspect ratio on the entropy generation rate due to fluid friction and heat transfer in the fluid. Results show that effect of inlet port height on the flow field is significant and entropy generation rate due to fluid friction is affected considerably by the inlet port height. The porosity lowers entropy generation rate due to fluid friction and heat transfer. It is found also that the effect of block aspect ratio on entropy generation rate is notable; in which case, entropy generation rate increases for the block aspect ratio of 1:2.

Mukhopadhyay (2010) investigated the entropy generation due to natural convection in a square cavity with multiple discrete heat sources. The effects of Rayleigh number, heater spacing, length and strength ratios of heaters were investigated. They found that minimum entropy generation rate was achieved for the same condition at which the minimum peak heater temperature was obtained. Cheng and Ma (1994) presented a numerical study of

entropy generation for mixed convection flow in a vertical channel with transverse fin arrays. They proposed an optimal geometrical configuration of the finned channel, which offers higher second-law efficiency. Shahi *et al.* (2011) numerically simulated the natural convection of a nanofluid in a cavity with a protruded heat source. The effect of Rayleigh number, solid concentration and heat source location on entropy generation were considered. The results have shown the maximum value of Nusselt number and minimum entropy generation are obtained when heat source mountains on the bottom horizontal wall. Kaluri and Basak (2011) presented the role of entropy generation on thermal management during natural convection in porous square cavities with distributed heat sources.

In the present study, a numerical study of forced convection heat transfer in a horizontal channel containing blocks using the entropy generation minimization method (EGM) is presented. The aim of this work is to investigate the evolution of the variation of entropy generation through the study of the effects of Reynolds number (Re), separation distance (S), height (C) and width (W) of the components on the flow structure and heat transfer inside the channel. The entropy generation minimization method (EGM) is applied to optimize geometrical configuration, fluid flow and heat transfer. The isotherms, streamlines and local entropy generation maps are plotted. The variation of the mean Nusselt number and the variation of the total entropy generation due to heat transfer and fluid friction irreversibilities versus Reynolds number, separation distance, height and width of the components are presented in graphical forms.

## 2. MODEL CONFIGURATION AND MATHEMATICAL FORMULATION

The configuration of the problem is depicted in Fig. 1. The geometric parameters considered in the dimensionless value are as follows:  $L_{in}=2$ ,  $L_{out}=4$ ,  $C=W=S=0.25$ ,  $H=1$  and  $L=6.75$ . A forced convection heat transfer is studied in a horizontal channel with length  $l$  and height  $H$ . Two identical heat sources are mounted on the bottom wall channel with length  $w$  and height  $c$  and spaced with  $s$  between them. The heating components are kept isothermal, at uniform temperature  $T_s$ . The first heat source is located at a distance  $l_{in}$  from the channel entrance. The flow is assumed to be steady, incompressible, and two-dimensional. At the channel inlet, a uniform fluid velocity  $U_0$  and temperature  $T_0$  were imposed.

The conservation equations of mass, momentum, and energy for a two-dimensional laminar forced convection, steady and incompressible flow, using the following dimensionless variables are:

$$X = \frac{x}{H}, \quad Y = \frac{y}{H}, \quad U = \frac{u}{U_0}, \quad V = \frac{v}{U_0},$$

$$\Theta = \frac{T-T_0}{T_s-T_0}, \quad P = \frac{p}{\rho_f U_0^2}, \quad v^* = \frac{\nu}{\nu_f}$$

Continuity

$$\frac{\partial U}{\partial X} + \frac{\partial V}{\partial Y} = 0 \tag{1}$$

X-momentum

$$U \frac{\partial U}{\partial X} + V \frac{\partial V}{\partial Y} = -\frac{\partial P}{\partial X} + \frac{1}{Re} \left\{ \frac{\partial}{\partial X} \left( v^* \frac{\partial U}{\partial X} \right) + \frac{\partial}{\partial Y} \left( v^* \frac{\partial U}{\partial Y} \right) \right\} \tag{2}$$

momentum

$$U \frac{\partial V}{\partial X} + V \frac{\partial V}{\partial Y} = -\frac{\partial P}{\partial Y} + \frac{1}{Re} \left\{ \frac{\partial}{\partial X} \left( v^* \frac{\partial V}{\partial X} \right) + \frac{\partial}{\partial Y} \left( v^* \frac{\partial V}{\partial Y} \right) \right\} \tag{3}$$

Where,

$$v^* = \begin{cases} \nu_s/\nu_f \rightarrow \infty & \text{in each heat source} \\ 1 & \text{in the fluid} \end{cases}$$

Energy

$$U \frac{\partial \Theta}{\partial X} + V \frac{\partial \Theta}{\partial Y} = \frac{1}{Re Pr} \left\{ \frac{\partial}{\partial X} \left( k^* \frac{\partial \Theta}{\partial X} \right) + \frac{\partial}{\partial Y} \left( k^* \frac{\partial \Theta}{\partial Y} \right) \right\} \tag{4}$$

Where,

$$k^* = \begin{cases} k_s/k_f \rightarrow \infty & \text{in each heat source} \\ 1 & \text{in the fluid} \end{cases}$$

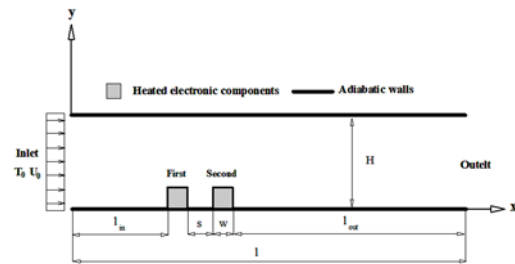


Fig. 1. A schematic diagram of the problem.

$U$  and  $V$  are dimensionless velocity components in the X- and Y- directions, respectively.  $Re$  represents the Reynolds number, and  $Pr$  the Prandtl number.  $\nu_s$  and  $\nu_f$  are the kinematic viscosities of the heat source and of the fluid (air), respectively, and  $v^* \rightarrow \infty$  in order to obtain  $U=V=0$  in a level of each heat source.  $k_s$ ,  $k_f$  are the thermal conductivities of the heat sources and the fluid (air), respectively, and  $k^* \rightarrow \infty$  in order to obtain a uniform temperature in a level of each heat source.

The dimensionless boundary conditions for our study are:

At  $X=0$  and  $0 \leq Y \leq H$ ,  $U=1$ ,  $V=0$ ,  $\Theta=0$  inlet channel  
 At  $X=L$  and  $0 \leq Y \leq H$ ,  $\frac{\partial U}{\partial X} = 0$ ,  $\frac{\partial V}{\partial X} = 0$ ,  $\frac{\partial \Theta}{\partial X} = 0$  outlet channel

$$\tag{5}$$

At  $Y=0$  and  $0 \leq X \leq L$ ,  $U=0$ ,  $V=0$ ,  $\frac{\partial \Theta}{\partial X} = 0$  adiabatic wall

$$\tag{5}$$

At  $Y=H$  and  $0 \leq X \leq L$ ,  $U=0$ ,  $V=0$ ,  $\frac{\partial \Theta}{\partial X} = 0$  adiabatic wall

The local total volumetric entropy generation in flow due to the heat transfer and fluid friction can be written as:

$$S_i = S_{i,h,t} + S_{i,f,f} \tag{6}$$

Where,

$$S_{\text{ht}} = \frac{k_f}{T_0^2} \left[ \left( \frac{\partial T}{\partial x} \right)^2 + \left( \frac{\partial T}{\partial y} \right)^2 \right] \quad (7)$$

And

$$S_{\text{fff}} = \frac{\mu}{T_0} \left[ 2 \left( \frac{\partial u}{\partial x} \right)^2 + 2 \left( \frac{\partial v}{\partial y} \right)^2 + \left( \frac{\partial u}{\partial x} + \frac{\partial v}{\partial y} \right)^2 \right] \quad (8)$$

These dimensionless equations can be written as follows:

$$S_{\text{ht}}^* = \left[ \left( \frac{\partial \theta}{\partial X} \right)^2 + \left( \frac{\partial \theta}{\partial Y} \right)^2 \right] \quad (9)$$

$$S_{\text{fff}}^* = \phi \left[ 2 \left( \frac{\partial U}{\partial x} \right)^2 + 2 \left( \frac{\partial V}{\partial y} \right)^2 + \left( \frac{\partial U}{\partial x} + \frac{\partial V}{\partial y} \right)^2 \right] \quad (10)$$

Where  $\phi$  is called the irreversibility distribution ratio, (which is the ratio of entropy generated due to fluid friction to entropy generated due to heat transfer), may be written as follows:

$$\phi = \frac{\mu T_0}{k} \left( \frac{U_0}{\Delta T} \right)^2 \quad (11)$$

With  $\Delta T = T_s - T_0$

Thus, the dimensionless local total entropy generation  $S^*$  is defined as follows:

$$S^* = \left[ \left( \frac{\partial \theta}{\partial x} \right)^2 + \left( \frac{\partial \theta}{\partial y} \right)^2 \right] + \phi \left[ 2 \left( \frac{\partial U}{\partial x} \right)^2 + 2 \left( \frac{\partial V}{\partial y} \right)^2 + \left( \frac{\partial U}{\partial x} + \frac{\partial V}{\partial y} \right)^2 \right] \quad (12)$$

The dimensionless total entropy generation is obtained by integrating the dimensionless local total entropy generation over the system volume:

$$S_T^* = \int_V S^* dv \quad (13)$$

The Bejan non-dimensional number  $Be$  is defined as follows:

$$Be = \frac{S_{\text{ht}}^*}{S_T^*} \quad (14)$$

Where,  $S_{\text{ht}}^*$ : dimensionless total entropy generation due to the heat transfer.  $S_T^*$ : dimensionless total entropy generation. When  $Be > 1/2$ , the irreversibility due to heat transfer dominates. For  $Be < 1/2$  the irreversibility due to the viscous effect dominates. For  $Be = 1/2$  heat transfer and fluid friction entropy generation are equal.

It may be noted that the effect of viscous dissipation is neglected in the energy equation (Eq. (4)), but that is considered for estimation of  $S_{\text{fff}}^*$

### 3. NUMERICAL PROCEDURE

The governing equations (1-4) were solved using a finite volume method (Patankar 1980). Scalar quantities ( $P$  and  $\Theta$ ) are stored at the center of these volumes, whereas the vectorial quantities ( $U$  and  $V$ ) are stored on the faces. The governing equations were discretized using the power-law scheme. The viscosity and thermal conductivity at the solid-fluid interface were determined by harmonic averaging. The SIMPLER algorithm (Patankar 1980) was used to determine the pressure from continuity equation. The discretized algebraic equations are solved by the line-by-line

tri-diagonal matrix algorithm (TDMA). Convergence is obtained when the maximum relative change between two consecutive iteration levels fell below than  $10^{-4}$  for  $U$ ,  $V$  and  $\Theta$ . Calculations were carried out on a PC with a 3.2 GHz CPU.

### 4. RESULTS AND DISCUSSION

Four effects of Reynolds number, separation distance, height and width of the components on the flow structure and heat transfer inside the channel were investigated. The entropy generation analysis is adopted in order to estimate the irreversibilities of the system during the electronic cooling process.

\*The Reynolds effect ( $Re$ ) is investigated through the correspond values of Reynolds numbers:  $Re=20, 50, 100$  and  $200$ .

\*The effect of the separation distance ( $S$ ) is investigated through the correspond values of separation distance:  $S= 0.25, 0.5, 0.75$  and  $1$ .

\*The effect of the height of the components ( $C$ ) is investigated through the correspond values of height of the components:  $C= 0.1, 0.2, 0.25$  and  $0.3$ .

\*The effect of the width of the components ( $W$ ) is investigated through the correspond values of width of the components:  $W= 0.1, 0.2, 0.25$  and  $0.3$ .

After the study of ( $Re, S, C, W$ ) effects, an optimization procedure of the geometric parameters, fluid flow and heat transfer within the channel containing heat sources is achieved. This procedure based on entropy minimization entropy (EGM) method, has for objective to determine:

- Optimal separation distance  $S_{\text{opt}}$ , for  $S=(0.25, 0.5, 0.75, 1, 1.5$  and  $2)$  and  $Re=(50,100$  and  $200)$ .
- Optimal height of heat source  $C_{\text{opt}}$ , for  $C=(0.1, 0.2, 0.25, 0.3, 0.4$  and  $0.5)$  and  $Re=(50,100$  and  $200)$ .
- Optimal width of heat source  $W_{\text{opt}}$ , for  $W=(0.1, 0.2, 0.25, 0.3, 0.4$  and  $0.5)$  and  $Re=(50,100$  and  $200)$ .
- Optimal configuration.

#### 4.1 Grid independence Study

To test and assess the grid independent solutions, five non-uniform grids are used:  $220 \times 72, 250 \times 82, 260 \times 92$  and  $280 \times 92$  nodes, for  $Re= 100$  and  $k_s/k_f \rightarrow \infty$  ( $T_s=\text{constant}$ ). The results of the grid variation study are presented in Table 1. Based on the results, of which the  $260 \times 92$  grid is adopted for all computations, because it gives us the best compromise between result accuracy and computing time.

#### 4.2 Code Validation

In order to verify the accuracy of the present

numerical study, the numerical code was validated by comparing our results with the numerical results of Davalath and Bayazitoglu (1987), Magherbi *et al.* (2003).

**Table 1 Results of the grid independence tests. Num1 and Num2 are the mean Nusselt numbers for the first and second component, respectively. Num is the mean Nusselt number for both components**

Grid	220×72 nodes	250×82 nodes	260×92 nodes	280×92 nodes
Num1	4.399	4.241	4.109	4.109
Num2	2.036	1.902	1.809	1.788
Num	6.435	6.144	5.919	5.898

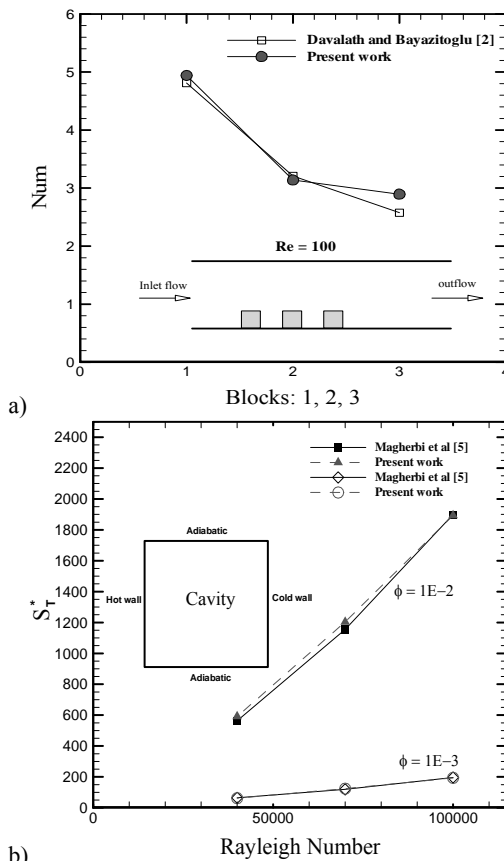


**Fig. 2. Comparison between our numerical results and predictions of Davalath and Bayazitoglu (1987) and Magherbi *et al.* (2003). (a) mean Nusselt number for each block, (b) dimensionless total entropy generation.**

For Davalath and Bayazitoglu (1987), a comparison of mean Nusselt number, for the forced convection Cooling in a horizontal channel containing three blocks, for Re=100. For Magherbi *et al.* (2003), a

comparison of dimensionless total entropy generation for the transient laminar natural convection of air in a rectangular cavity. The horizontal walls are insulated, while the vertical walls are kept at different temperatures. As shown in Fig 2, it is clear that the numerical results of the present work are in a good agreement with Davalath and Bayazitoglu (1987), Magherbi *et al.* (2003).

### 4.3 Effect of the Reynolds Number Re

To investigate the effect of Reynolds number on the fluid flow, heat transfer and entropy generation within the channel, simulations have been accomplished for Re= 20, 50, 100, and 200. The parameters kept constant in this section are: W=0.25, S=0.25, C=0.25 and  $\Delta T=T_s-T_0=40K$ , ( $T_s$  is the temperature of the heat source and  $T_0$  is the inlet temperature).

Figure 3 shows the variation of the mean Nusselt number with the Reynolds number. We remark that with increasing of Reynolds number, the mean Nusselt number increases. As a result, a good cooling of electronic components is obtained with increasing the Reynolds number, i.e. with increasing the fan energy.

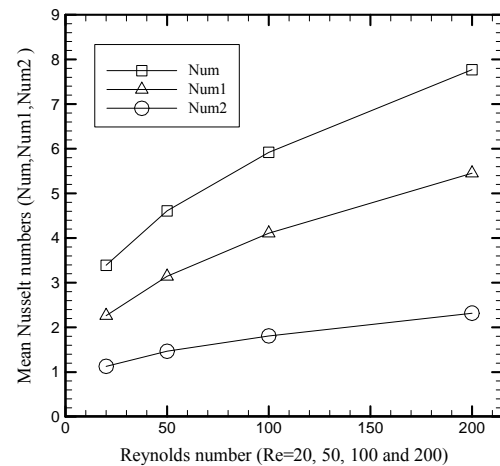


**Fig. 3. Mean Nusselt numbers as a function of Reynolds number. Here, Num is the mean Nusselt number for both components, Num1 and Num2 are the mean Nusselt numbers for the first and second component, respectively.**

Figures 4a-c present the variation of the dimensionless total entropy generation as a function of the Reynolds number.

The total entropy generation increases with increase the Reynolds number. In this case, the increase of the Reynolds number promotes the heat transfer in the channel, but increases the irreversibilities in the fluid. As seen in Figures 4b and 4c, we remark that the heat transfer irreversibility is predominant on the fluid friction irreversibility. This result can be explained by a high thermal gradients superior to the weak velocity gradients, caused by the low values of Reynolds numbers (Re= Re= 20, 50, 100, and 200) and by the very low value of the air viscosity.

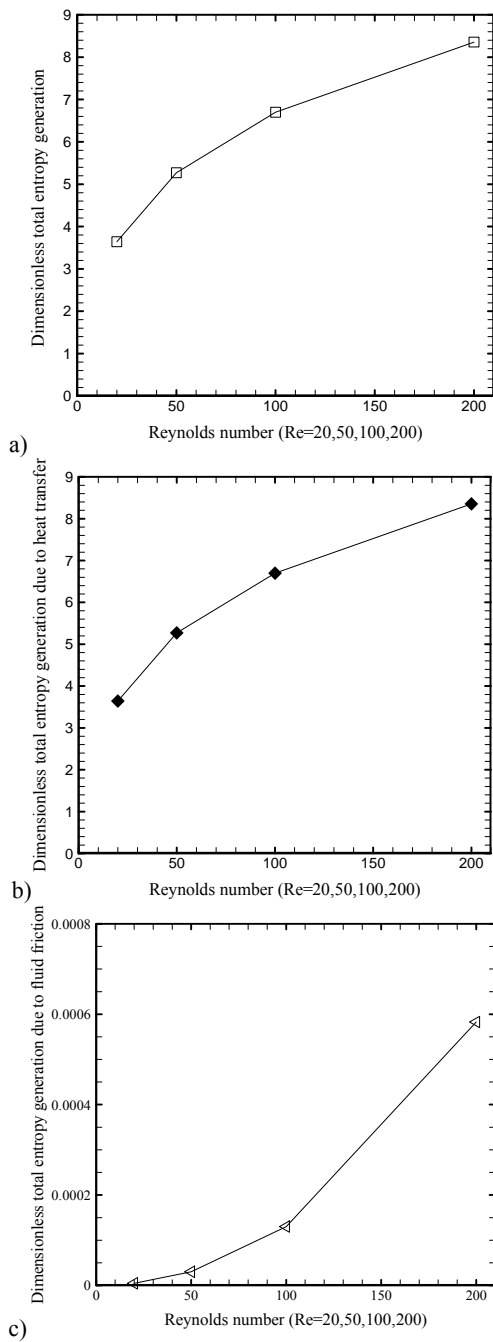


**Fig. 4. Dimensionless total entropy generation as a function of Reynolds number. (a) Dimensionless total entropy generation, (b) Dimensionless total entropy generation due to heat transfer and (c) Dimensionless total entropy generation due to fluid friction.**

Figure 5 illustrates the dimensionless local total entropy generation (due to the fluid friction and the heat transfer) contours for different Reynolds numbers. We note that the main source of the irreversibility of the system (fluid) and the degradation of its energy are the heat sources, because the region localized around them contains the maximal values of the total entropy generation. Far from the blocks, the total entropy generation decreases until to reach null values at the entry of the

channel, from where the velocity and thermal gradients are negligible. For  $Re=20$ , the contours of the local total entropy generation essentially occupy a part of the channel, that includes the two heat sources. By increasing the Reynolds number ( $Re=20$  to 200), this part grew in length and spreads horizontally in the sense of the fluid flow, while occupying more places in the channel domain. This result shows well that the increase of the Reynolds number, increases the irreversibility of the system, and so decreases its performances. The increase of irreversibilities is due to the increase of the temperature and velocity gradients. We remark also that the total entropy generation remains constant between the heat sources, even though we increase the Reynolds number.

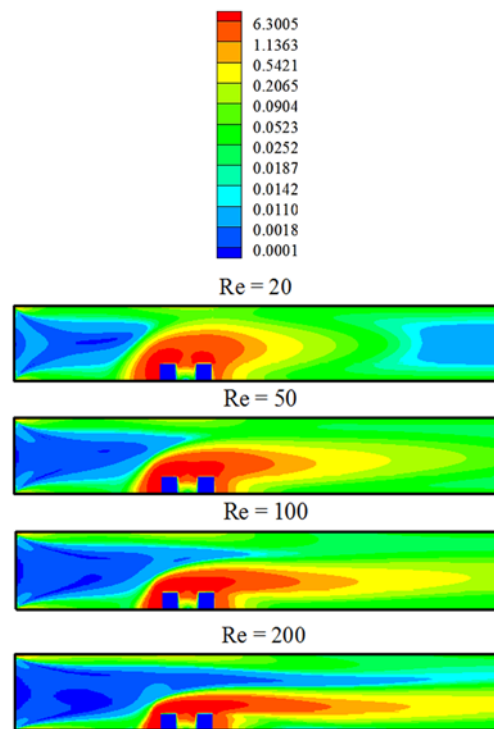


**Fig. 5. Contours of dimensionless local total entropy generation as a function of Reynolds number.**

Also seen, the total entropy generation close the first heat source is higher than the second, because the first block is better cooled than the second ( $Num1 > Num2$ , see Fig. 3), and thus, the thermal and velocity gradients near the first heat source are higher than in the second heat source.

Figures 6a-b illustrate the streamline and isotherm contours for different Reynolds numbers, respectively. By increasing the Reynolds number, two recirculation zones are created. The size of the recirculation zones increases and the recirculation zone downstream of the second block increases in length. The formation of recirculation zones prevents air to enter into the bottom portions between the blocks and after the second block, what gives a bad cooling for the second block and between the both blocks, in relation to the first block. As a

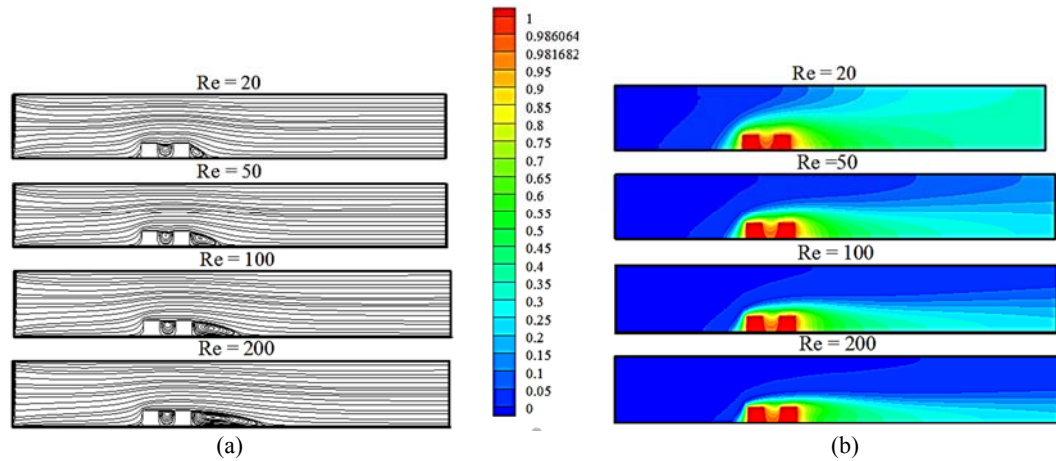


Fig. 6. (a) Streamlines and (b) isotherms as a function of Reynolds number.

result, a temperature gradient in the first component is higher than in the second and between them. Also, because the temperature stagnates between the both heat sources, caused by the recirculation zone with a constant size, a constant heat transfer is noticed, and then, a constant total entropy generation is obtained. As seen in Figure 6b, when increasing Reynolds number, the isotherms become approximately horizontal and a good heat removal is obtained.

Figure 7 presents the Bejan number with Reynolds numbers. We note that the Bejan number remains constant  $Be=1$ , in spite of the increase of Reynolds number. Bejan number equal one ( $Be=1$ ) shows that the effect of the heat transfer irreversibility is indeed dominant on the effect of viscous irreversibility, as seen in Figs. 4b and 4c. This result is caused by the low value of the viscosity of the fluid (Air) and by the low fluid velocities ( $Re=20, 50, 100$  and  $200$ ). However, the fluid flow creates the irreversibility of the system by a convective heat transfer, in spite of the low flow velocities.

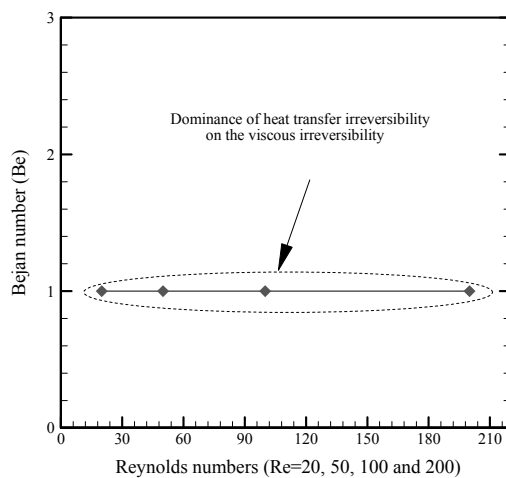


Fig. 7. Bejan number as a function of Reynolds number.

At the end, we can say that the effect of the fluid

friction on the entropy generation is insignificant. So, we can confirm that the term of the viscous dissipation can be neglected in this problem.

#### 4.4 Effect of the Separation Distance S

To examine the effect of separation distance parameter on the flow structure, heat transfer and entropy generation, we varied this parameter by taking the following values:  $S=0.25, 0.5, 0.75$  and  $1$ . The parameters kept constant in this section are:  $Re=100, W=0.25, C=0.25$  and  $\Delta T=T_s - T_0 = 40K$ .

Figure 8 presents the variation of the mean Nusselt number as a function of the separation distance. We remark that while increasing of separation distance, the mean Nusselt number increases. We conclude that the increase of the separation distance improves the heat sources cooling. Therefore, increasing the separation distance, causes an increase in the total entropy generation, and creates the irreversibilities in the system, and so reduces its performances (see Fig. 9).

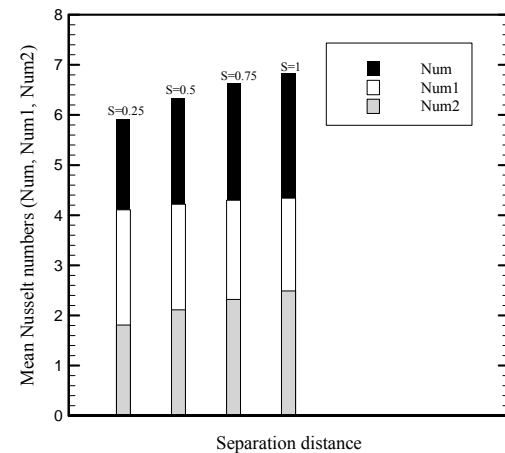
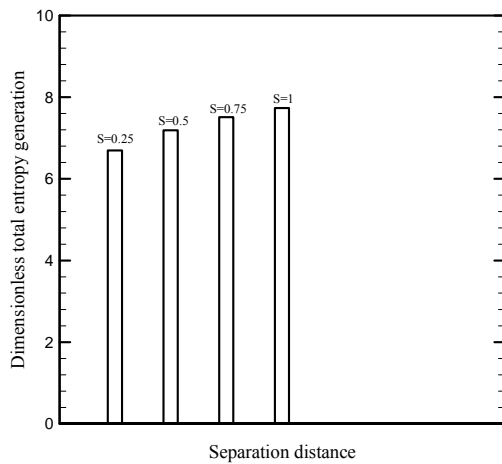
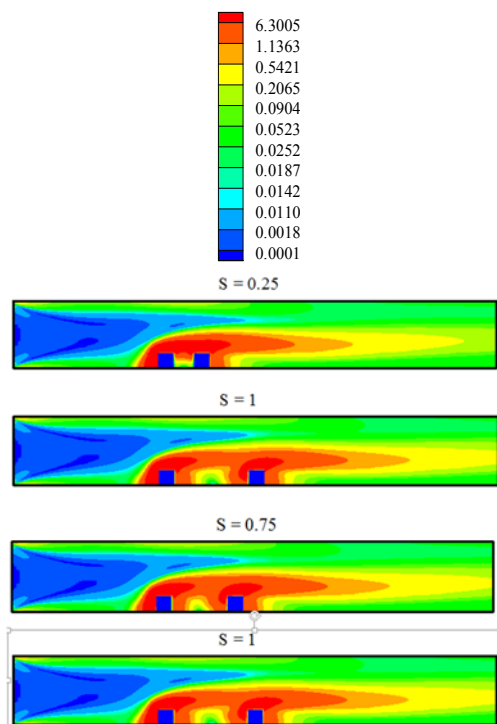


Fig. 8. Mean Nusselt numbers as a function of separation distance. Here, Num is the mean Nusselt number for both components, Num1 and Num2 are the mean Nusselt numbers for the first and second component, respectively.



**Fig. 9. Dimensionless total entropy generation as a function of separation distance.**



**Fig. 10. Contours of dimensionless local total entropy generation as a function of separation distance.**

Figure 10 illustrates the dimensionless local total entropy generation (due to the fluid friction and the heat transfer) contours for different separation distances. We note that the maximal values of the total generation entropy are situated in the zone close to the heat sources. However, the low values of the total generation entropy are essentially localized at the entrance channel and far from the heat sources, because of the low thermal and velocity gradients. As we increase the distance that separates the two heat sources, the total entropy generation becomes significant in this separation zone. This is due to the increase of the convective heat transfer, because the airflow penetrates easily in this zone, what is going to increase the velocity and thermal gradients. Also, by spacing the two heat sources, their influences on

the heat transfer inside the channel become considerable, and the contours of the local total entropy generation spread horizontally in the downstream of the second heat source and occupy more places in the channel domain.

Figure 11 presents the isotherm contours for different separation distances. We observe that while moving away the both heat sources, the thermal gradient increases between the heat source and the separation zone increases. Thus, the increase of the thermal gradient increases the total entropy generation in the separation zone. Therefore, the thermal gradient and total entropy generations remain constant in the upstream of the first heat source and just downstream of the second heat source, what explains a constant total entropy generation in these zones (see Fig. 10).

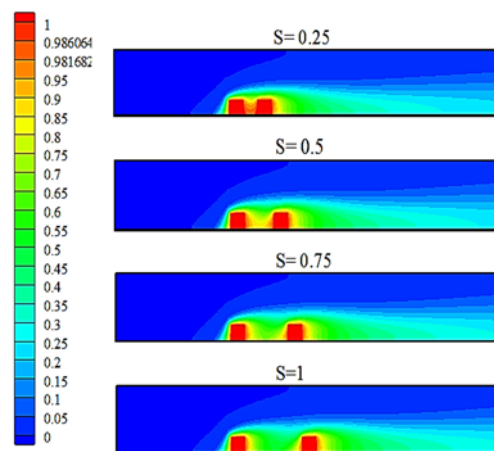


**Fig. 11. Isotherms as a function of separation distance.**

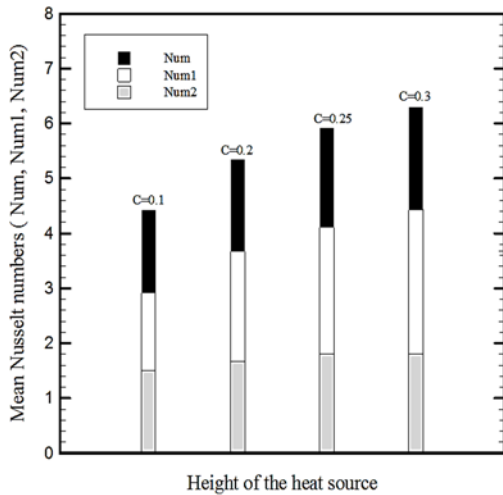
#### 4.5 Effect of the Height of the Components C

The effect of the height of the components on the fluid flow, heat transfer and entropy generation is studied by carrying out a series of calculations for different heights of the component:  $C=0.1, 0.2, 0.25$  and  $0.3$ . The parameters kept constant in this section are:  $Re=100, S=0.25, W=0.25$  and  $\Delta T=T_s - T_0 = 40K$ .

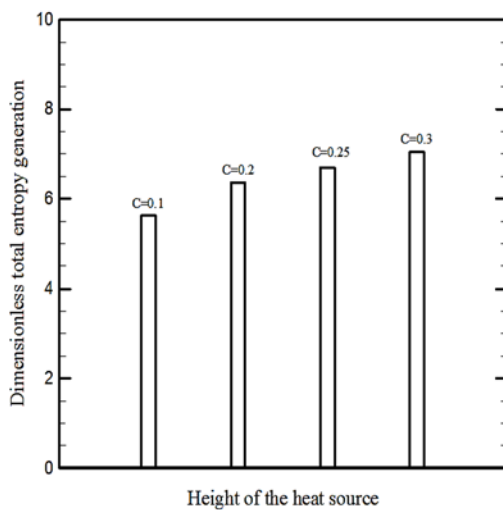
Figure 12 presents the variation of the mean Nusselt number as function of the height of heat source. With increasing the height of the both components, the Nusselt number increases. In this case, we can confirm that the heat sources are better cooled, even though we increase their height. We observed also that the first block is better cooled than the second, in spite of the variation of the height of heat source. However, to change the size of heat sources, by increasing their heights, increases the entropy generation, and creates irreversibilities in the system (see Fig. 13).

Figure 14 illustrates the dimensionless local total entropy generation contours for different heights of heat sources. We can see that the maximal values of total entropy generation are situated in the regions close to the both components. This is due to the higher thermal gradients generated by the heat sources in these regions. Also seen, for the case  $C=0.1$ , the separation zone contains practically the

maximal values of total entropy generation in relation to the other cases ( $C=0.2, 0.25$  and  $0.3$ ), what is going to increase the irreversibilities in this zone. We remark also that while increasing the height of the heat source, the distribution of the total entropy generation enlarges into the channel, downstream and above both components.



**Fig. 12.** Mean Nusselt numbers as a function of the height of heat source. Here, Num is the mean Nusselt number for both components, Num1 and Num2 are the mean Nusselt numbers for the first and second component, respectively.



**Fig. 13.** Dimensionless total entropy generation as a function of the height of heat source.

Figure 15 present the isotherm contours for different heights of heat sources. In the separation zone between the heat sources, the heat transfer is better in the case  $C=0.1$  than for the others cases ( $C=0.2, 0.25$  and  $0.3$ ). Therefore, Also, for the case  $C=0.1$ , the height of the heat source is smaller than for the others cases ( $C=0.2, 0.25$  and  $0.3$ ), that occupy more place in the channel domain, and have a bigger surface heat exchange, that allows them to enhance the heat transfer, and creates irreversibilities inside the channel, than in the case of  $C=0.1$ .

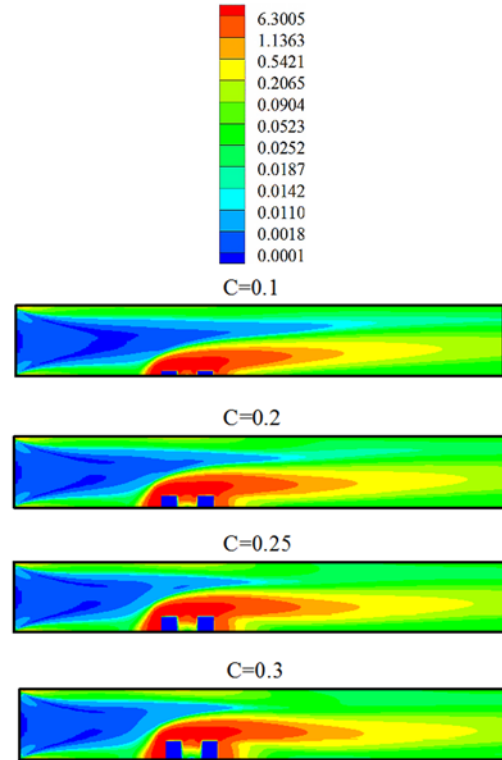


**Fig. 14.** Contours of dimensionless local total entropy generation as a function of the height of heat source.

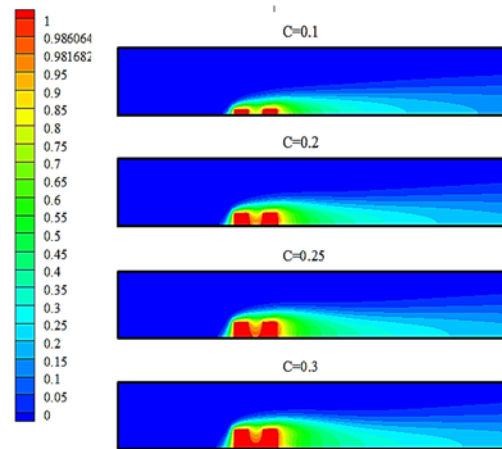


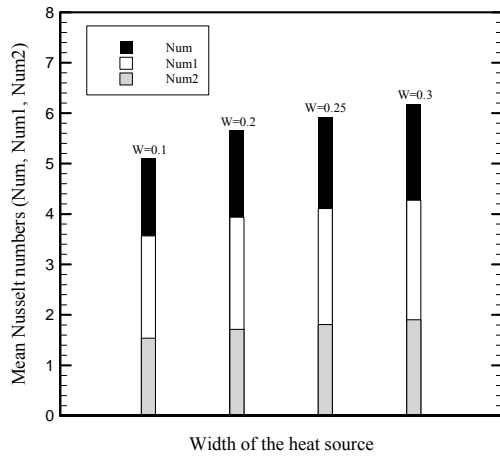
**Fig. 15.** Isotherms as a function of the height of heat source.

#### 4.6 Effect of the Width of the Components W

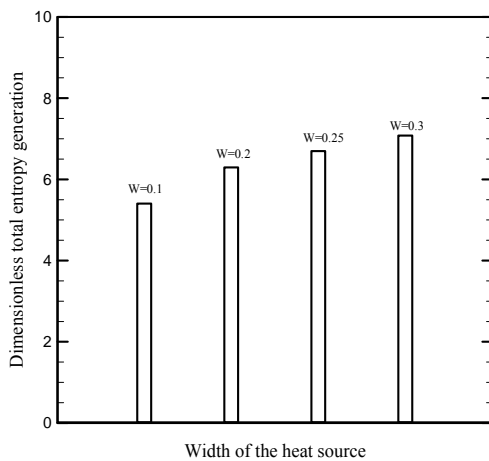
In order to study the influence of the width of the components on the fluid flow, heat transfer and entropy generation in the channel, the width of the components will be changed by opting for the following values:  $W=0.1, 0.2, 0.25$  and  $0.3$ . The parameters kept constant in this section are:  $Re=100, S=0.25, C=0.25$  and  $\Delta T=T_s - T_0=40K$ .

Figure 16 shows the variation of mean Nusselt number as a function of the width of the block. We remark that increasing the width of the blocks, increases the mean Nusselt number and encourages the cooling of the components. We remark also that the first block is better cooled than the second

(Num1>Num2), in spite the increase of the width of the blocks. Therefore, the increase of the width of the blocks, increases the total entropy generation, and reduces the performance of the system, (see figure 16).



**Fig. 16. Mean Nusselt numbers as a function of the width of heat source.** Here, Num is the mean Nusselt number for both components, Num1 and Num2 are the mean Nusselt numbers for the first and second component, respectively.



**Fig. 17. Dimensionless total entropy generation as a function of the width of heat source.**

To analyze this result, we examine the Fig. 18, that present the contours of the dimensionless local total entropy generation for different widths of the component. Based on the analysis of previous effects (effects of Re, S and C), we conclude that the main source of irreversibilities of the system are the both heat sources. Because, if we increase the width of the heat source (W=0.1 to 0.3), the size of heat source takes more places in the channel domain, and have more influence in the increase of the total entropy generation inside the channel. We remark also, that in spite of the variation of the width of heat source, the total entropy generation remains constant in the upstream of the first heat source, between the both heat sources and just downstream of the second heat source. Therefore, the total entropy generation

increases above the both components, with increasing the width of heat sources.

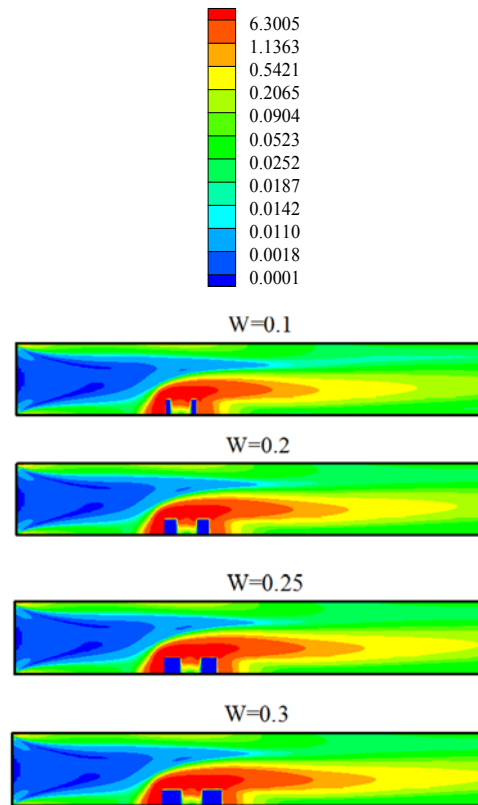


**Fig. 18. Contours of dimensionless local total entropy generation as a function of the width of heat source.**

This result can be explained by the analysis of the Fig. 19 that shows the isotherm contours, for different widths of heat source. To increase the width of heat source, increase the top heat surface exchange of heat source, and thus, increase the thermal gradient above of both heat sources, and thus, increase the total entropy generation. We can also see that the constant heat transfer existing upstream the first heat source, between the both heat sources and just after the second heat source gives a constant total entropy generation.

#### 4.7 Optimization Procedure

The procedure of optimization of geometrical parameters (S, C, and W), fluid flow (Re) and heat transfer (Num) is based on two following essential criterias:

- A maximal value of mean Nusselt number, i.e. a best cooling of both heat sources.
- A minimal value of total generation entropy, i.e. a minimal value of the loss of the system energy.

To satisfy these two criteria's, we consider a global criteria named the optimization factor "η", that is defined by the following relation:

$$\eta = \frac{\text{Num}}{S_T^*} \quad (15)$$

**Table 2 Mean Nusselt number, total entropy generation and optimization factor as a function of separation distance (S=0.25, 0.75, 1, 1.5 and 2) and Reynolds number (Re=50,100 and 200)**

C	W	S	Re=50			Re=100			Re=200		
			Num	$S_T^*$	$\eta$	Num	$S_T^*$	$\eta$	Num	$S_T^*$	$\eta$
0.25	0.25	S=0.25	4.608	5.27	0.874	5.919	6.697	0.883	7.772	8.352	0.93
-	-	S=0.5	4.955	5.662	0.875	6.333	7.19	0.88	8.297	8.974	0.924
-	-	S=0.75	3.807	5.921	0.643	6.620	7.513	0.881	8.673	9.394	0.923
-	-	S=1.0	6.1	5.378	1.134	6.831	7.735	0.883	8.946	9.67	0.925
-	-	S=1.5	5.819	6.317	0.921	5.491	8.171	0.672	9.548	9.98	0.956
-	-	S=2.0	6.123	6.436	0.951	5.890	8.3	0.71	10.067	10.2	0.987

$\eta$ : is defined as the ratio of Nusselt number to the total entropy generation.

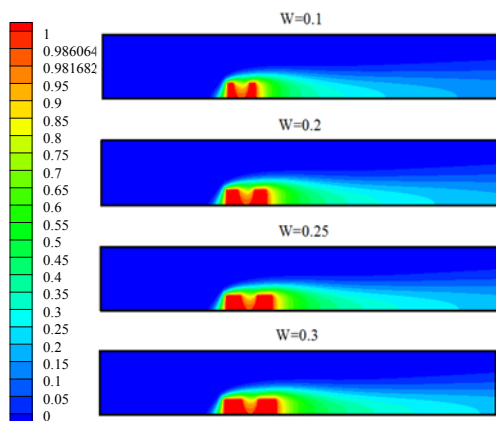


**Fig. 19. Isotherms as a function of the width of heat source.**

We note that the optimal condition is for an increase of optimization factor i.e. an increase of the Nusselt number (Num) and a decrease of the total entropy generation ( $S_T^*$ ). This procedure has significance in the cooling process of electronic components.

In this section, we are going to try to determine:

Optimal separation distance  $S_{opt}$ .

Optimal height of heat source  $C_{opt}$ .

Optimal width of heat source  $W_{opt}$ .

Optimal configuration.

#### 4.7.1 Optimal Separation Distance $S_{opt}$

Table 2 shows mean Nusselt number, total entropy generation and optimization factor as a function of separation distance (S=0.25, 0.75, 1, 1.5 and 2) and

Reynolds number (Re=50,100 and 200). The parameters kept constant in this section are: C=0.25, W=0.25 and  $\Delta T=T_s - T_0=40K$ .

For Re=50 and 100, when S increases, the optimization factor  $\eta$  increases until to reach a maximal value, then it falls to a lower value. The increase of  $\eta$  is due to the increase of Nusselt number i.e. an improvement of the cooling of heat sources, and also due to the diminution of total entropy generation i.e. a reduced loss of the fan energy in the channel. For Re=200, when S increases,  $\eta$  is approximately constant and close to 1. This result shows an equality between the Nusselt number and total entropy generation i.e. a better cooling of components causing a considerable energy loss for Re=50 and 100. The optimal separation distance  $S_{opt}$  is obtained by comparing  $\eta$  between Re=50, 100 and 200. We conclude that the optimal separation distance between the both heat sources  $S_{opt}$  is for higher  $\eta$  ( $\eta=1.134$ ), situated at:  $S_{opt}=1$  with W=0.25, C=0.25 and Re=50.

#### 4.7.2 Optimal Height of Heat Source $C_{opt}$

Table 3 shows mean Nusselt number, total entropy generation and optimization factor as a function of height of heat source (C=0.1, 0.2, 0.25, 0.3, 0.4 and 0.5) and Reynolds number (Re=50,100 and 200). The parameters kept constant in this section are: S=0.25, W=0.25 and  $\Delta T=T_s - T_0 =40K$ .

For Re=50, 100 and 200, when we increase the height of the heat source, the optimization factor  $\eta$  increase until a maximal value, then it falls to a lower value. For Re=50 and 200, the total entropy generation is very higher than the Nusselt number for all height values of heat source.

Therefore, for Re=100, a small difference between the Nusselt number and the generation of entropy, except for C=0.4 C=0.5, from where the total entropy

**Table 3 Mean Nusselt number, total entropy generation and optimization factor as a function of height of heat source (C=0.1, 0.2, 0.25, 0.3, 0.4 and 0.5) and Reynolds number (Re=50,100 and 200)**

S	W	C	Re=50			Re=100			Re=200		
			Num	$S_T^*$	$\eta$	Num	$S_T^*$	$\eta$	Num	$S_T^*$	$\eta$
0.25	0.25	C=0.1	2.613	4.4	0.594	4.421	5.624	0.786	4.312	7.145	0.603
-	-	C=0.2	3.00	5.01	0.598	5.347	6.368	0.84	7.00	7.982	0.877
-	-	C=0.25	4.608	5.27	0.874	5.919	6.698	0.883	5,413	8,469	0.639
-	-	C=0.3	3.34	5.565	0.600	6.302	7.037	0.895	5.524	8.88	0.622
-	-	C=0.4	3.374	6.173	0.546	4.341	8.164	0.531	5.685	9.8	0.58
-	-	C=0.5	3.574	6.908	0.517	4.675	9.27	0.504	6.19	11	0.562

**Table 4 Mean Nusselt number, total entropy generation and optimization factor as a function of width of heat source (W=0.1, 0.2, 0.25, 0.3, 0.4 and 0.5) and Reynolds number (Re=50,100 and 200)**

S	C	W	Re=50			Re=100			Re=200		
			Num	$S_T^*$	$\eta$	Num	$S_T^*$	$\eta$	Num	$S_T^*$	$\eta$
0.25	0.25	W=0.1	4.003	4.331	0.924	5.104	5.405	0.944	6.669	6.642	1.004
-	-	W=0.2	4.077	4.979	0.818	5.6525	6.297	0.897	7.412	7.823	0.947
-	-	W=0.25	4.608	5.270	0.874	5.9193	6.698	0.883	7.770	8.355	0.93
-	-	W=0.3	4.804	5.545	0.866	6.178	7.077	0.873	8.116	8.859	0.916
-	-	W=0.4	4.953	6.024	0.822	6.386	7.857	0.812	8.402	9.687	0.867
-	-	W=0.5	5.127	6.476	0.791	6.622	8.483	0.78	8.718	10.489	0.831

generation is very higher than the Nusselt number. This result shows that the optimal case for C is situated in the case of Re=100. By comparing  $\eta$  for all Reynolds numbers and heights of heat source, the optimal height of heat source is for higher  $\eta$  ( $\eta=0.895$ ), remarked at:  $C_{opt}=0.3$  with  $W=0.25$ ,  $C=0.25$  and  $Re=100$ .

**4.7.3 Optimal Width of Heat Source  $W_{opt}$**

Table 4 shows mean Nusselt number, total entropy generation and optimization factor as a function of width of heat source ( $W=0.1, 0.2, 0.25, 0.3, 0.4$  and  $0.5$ ) and Reynolds number ( $Re=50,100$  and  $200$ ).

The parameters kept constant in this section are:  $S=0.25, W=0.25$  and  $\Delta T=T_s- T_0=40K$ .

While varying C and Re, we notice that the optimization factor  $\eta$  takes its maximal value for  $W=0.1$ , then it decreases until to reach a lower value. In spite the increase of the Nusselt number, the diminution of  $\eta$  is essentially due to the increase of the total entropy generation, caused by the increase of the size of heat source i.e. by increasing its width. By comparing  $\eta$  for all Reynolds numbers and widths of heat source, the optimal height of heat source is for higher  $\eta$  ( $\eta=1.004$ ), observed at:  $W_{opt}=0.1$  with  $S=0.25, C=0.25$  and  $Re=200$ .

#### 4.7.4 Optimal Configuration

The optimal configuration of our physical problem is determined by a comparison of the optimization factor  $\eta$  between the optimal solutions, previously determined, that are:

$$S_{opt}=1, W=0.25, C=0.25, Re=50, \eta=1.134$$

$$C_{opt}=0.3, W=0.25, S=0.25, Re=100, \eta=0.895$$

$$W_{opt}=0.1, S=0.25, C=0.25, Re=200, \eta=1.004$$

We remark that:  $\eta S_{opt} > \eta C_{opt} > \eta W_{opt}$

Thus, the optimal and the best configuration for maximum heat transfer and minimum entropy generation is observed at:  $Re=50, S=1, C=0.25, W=0.25$ .

### 5. CONCLUSION

Forced convection air-cooling of two identical heat sources mounted in a horizontal channel is studied. Four effects of the Reynolds number, the separation distance, the height and the width of the components were considered. The entropy generation minimization method (EGM) is applied to optimize the heat transfer and fluid flow in the channel.

The main results of this study are:

- 1-The mean Nusselt number increases with increase of Reynolds number. Because of the low value of the viscosity of the fluid (Air) and the low fluid velocities ( $Re=20, 50, 100$  and  $200$ ), the effect of fluid friction on the entropy generation is insignificant. As a consequence, the term of the viscous dissipation can be neglected in this problem.
- 2-The mean Nusselt number and the total entropy generation increase with increase of separation distance, height and width of the components.
- 3-It is imperative to optimize the heat transfer and fluid flow in the channel, in order to reduce the loss of the fan energy and to promote the cooling of heat sources
- 4-The optimal values of separation distance, height and width heat source are, respectively:

$$S_{opt}=1, W=0.25, C=0.25, Re=50, \eta=1.134$$

$$C_{opt}=0.3, W=0.25, S=0.25, Re=100, \eta=0.895$$

$$W_{opt}=0.1, S=0.25, C=0.25, Re=200, \eta=1.004$$

- 5- The optimal and the best configuration for maximum heat transfer and minimum entropy generation is observed at:  $Re=50, S=1, C=0.25, W=0.25$ .

### REFERENCES

Abbassi, H., M. Magherbi and A. Ben Brahim (2003). Entropy generation in Poiseuille–Benard channel flow. *International Journal of Thermal Sciences* 42, 1081–1088.

Afrid, M. and A. Zebib (1989). Natural convection

cooling of heated components mounted on a vertical wall. *Numerical Heat Transfer Part A* 15, 243-259.

Balaji, C., M. Hölling and H. Herwig (2007). Entropy generation minimization in turbulent mixed convection flows. *International Communications in Heat and Mass Transfer* 34, 544–552.

Bejan, A. (1994). Entropy Generation through Heat and Fluid Flow. *John Wiley & Sons*.

Bensouici, M. and R. Bessaih (2010). Mixed Convection in a vertical channel with discrete heat sources using a porous matrix. *Numerical Heat Transfer Part A* 58, 581-604.

Cheng, C. H. and W. P. Ma (1994). Numerical predictions of entropy generation for mixed convective flows in a vertical channel with transverse fin array. *International Communications in Heat and Mass Transfer* 21, 519–530.

Dagtekin, I., H. F. Oztop and A. Bahloul (2007). Entropy generation for natural convection in  $\Gamma$ -shaped enclosures. *International Communications in Heat and Mass Transfer* 34, 502–510.

Davalath, J., and Y. Bayazitoglu (1987). Forced convection cooling across rectangular blocks. *ASME. Journal of Heat Transfer* 109, 321-328.

Jian-hui, Z., Y. Chun-xin and Z. Li-na (2009). Minimizing the entropy generation rate of the plate-finned heat sinks using computational fluid dynamics and combined optimization. *Applied Thermal Engineering* 29, 1872–1879.

Kaluri, R. S. and T. Basak (2011). Role of entropy generation on thermal management during natural convection in porous square cavities with distributed heat sources. *Chemical Engineering Science* 66, 2124–2140.

Magherbi, M., H. Abbassi and A. Ben Brahim (2003). Entropy generation at the onset of natural convection. *International Journal of Heat and Mass Transfer* 46, 3441–3450.

Mukhopadhyay, A. (2010). Analysis of entropy generation due to natural convection in square enclosures with multiple discrete heat sources. *International Communications in Heat and Mass Transfer* 37, 867–872.

Patankar, S.V. (1980). *Numerical Heat Transfer and Fluid Flow*, McGraw-Hill, New York.

Shahi, M., A. H. Mahmoudi and A.H.Raouf (2011). Entropy generation due to natural convection cooling of a nanofluid. *International Communications in Heat and Mass Transfer* 38, 972–983.

Shuja, S. Z., B. S.Yilbas and A. Jamal (2008). Entropy generation in flow field subjected to a porous block in a vertical channel. *Transport in Porous Media* 72, 179-197.

